This is a manuscript version of this paper. The paper was first published as:

Frost, Ray L. and Zhou, Qin and He, Hongping and Xi, Yunfei and Zbik, Marek (2007) TEM, XRD and thermal stability of adsorbed paranitrophenol on DDOAB organoclay . *Journal of Colloid and Interface Science* 311(1):pp. 24-37.

TEM, XRD and thermal stability of adsorbed paranitrophenol on DDOAB organoclay

Qin ZHOU [1,2,3], Ray L. FROST [2*], Hongping HE [1,2] , Yunfei Xi [2,4] and Marek Zbik[2]

[1] Guangzhou Institute of Geochemistry, Chinese Academy of Sciences, Guangzhou 510640, China

[2] Inorganic Materials Research Program, School of Physical and Chemical Sciences, Queensland University of Technology, GPO Box 2434, Brisbane, QLD 4001, Australia

[3] Graduate University of Chinese Academy of Sciences, Beijing 100039, China

[4] Centre for Environmental Risk Assessment & Remediation, University of South Australia, Mawson Lakes, SA, 5095, Australia

Abstract

Water purification is of extreme importance to modern society. Organoclays through adsorption of recalcitrant organics provides one mechanism for the removal of these molecules. The organoclay was synthesised through ion exchange with dimethyldioctadecylammonium bromide labeled as DDOAB of formula $(CH_3(CH_2)_{17})_2NBr(CH_3)_2$. Paranitrophenol was adsorbed on the organoclay at a range of concentrations according to the cation exchange capacity (CEC) of the host montmorillonite. The paranitrophenol in solution was analysed by a UV-260 spectrophotometer at 317nm, with detection limits being 0.05mg/L. The expansion of the montmorillonite was studied by a combination of X-ray diffraction and transmission electron microscopy. Upon adsorption of the paranitrophenol the basal spacing decreased. The thermal stability of the organoclay was determined by a combination of thermogravimetry and infrared emission spectroscopy. The surfactant molecule DDOAB combusts at 166, 244 and 304 °C and upon intercalation into Na-montmorillonite is retained up to 389 °C thus showing the organoclay is stable to significantly high temperatures well above the combustion/decomposition temperature of the organoclay.

Key words: adsorption, intercalation**,** montmorillonite, organo-clay, infrared spectroscopy, emission, paranitrophenol.

Introduction:

The production of potable water is of extreme importance world wide. Water may be contaminated with many organic molecules including hormones, pesticides and herbicides. Many of these molecules are recalcitrant and difficult to remove through oxidation or photocatalytic oxidation using for example hydrogen peroxide and intense UV radiation. One method for purifying water is to use organoclays [1-5]. These organoclays are prepared by ion exchange of the cation in the swelling clay such as montmorillonite with a cation surfactant [6-9]. Organoclays may be synthesised by ion exchange of the mono or divalent cations (For example Na^{+}, Mg^{2+} or Ca^{2+}) with a large organic cation such as dimethyldioctadecylammonium bromide labeled as DDOAB of formula $(CH_3(CH_2)_{17})_2NBr(CH_3)_2$. These cationic surfactants may consist of single, double or triple long chain alkyl chains. The surface properties of these organoclays change significantly from hydrophilic to hydrophobic/lipophilic. These clays then have useful properties for example the removal of oil from potable water, and other toxic chemicals and humic materials from water [10-12]. These modified clay minerals, organo-clays, represent a family of materials which have many applications in a range of key areas, such as adsorbents for organic pollutants [13, 14], rheological control agents [15], reinforcing fillers for plastics and electric materials [16-18].

The influence of montmorillonite surfaces on the chemical and physical properties of adsorbed H_2O molecules has been the subject of a number of recent studies using structural, thermodynamic, spectroscopic and computational methods. Generally, the position of the ν_2 mode of H_2O decreases and H_2O stretching band shifts to higher wavenumber upon lowering the H_2O content in cation-exchanged montmorillonite. At the same time, the cation type is determinative for total water content retained in clay minerals. However, to the best of our knowledge, there are few reports about the role of sorbed H_2O molecules in organo-clays and it is very important for the application of organo-clays. Hence, the situation of the sorbed H_2O molecules in organo-clays at different surfactant concentrations is discussed in this paper. Recently FTIR spectroscopy using ATR and KBr pressed disk techniques has been used to characterize sorbed water and $HDTMA^{+}$ in organo-clay [19, 20]. It was found that sorbed water content decreases with the intercalation of $HDTMA^{+}$. In this work we extend these studies to the changes in the surfactant upon intercalation and to the adsorption/absorption of a test molecule namely paranitrophenol on the organoclay. Infrared emission spectroscopy (IES) technique is used to study the changes in structure of the organo-clay formed between a montmorillonitic clay and dimethyldioctadecylammonium bromide and the adsorbed paranitrophenol.

Montmorillonites are widely used in a range of applications because of their high cation exchange capacity, swelling capacity, high surface areas, and consequential strong adsorption and absorption capacities [21-24]. These clay properties can be enhanced by converting the montmorillonite to an organoclay by ion exchange of the cation with a surfactant molecule [21, 25-27]. The hydration of inorganic cations on the exchange sites causes the clay mineral surface to be hydrophilic. Natural clays are thus ineffective sorbents for organic compounds. Modification of the montmorillonite clay with surfactant molecules changes the properties of the clay. The intercalation of

a cationic surfactant not only changes the surface properties from hydrophilic to hydrophobic but also greatly increases the basal spacing of the layers [21, 25-28].

Such surface property changes will effect the applications of the organoclay. In particular, the hydrophobic nature of the organoclay implies that the material can be used as a filter material for water purification through for example the removal of hydrocarbons and pesticides. Studies have shown that replacing the inorganic exchangeable cations of clay minerals with organic cations can result in a greatly enhanced capacity of these materials to remove organic contaminants [29, 30]. The adsorption properties of the organoclay strongly depend on the structure and molecular arrangements of the surfactant molecules within the organoclays . Understanding the structure and properties of synthesised organoclays is essential for their adsorption/absorption applications [8, 31-33].

Recently studies of organoclays with single alkyl chain surfactant molecules has been published [34]. The objective of this work is the study of the adsorption of the paranitrophenol on an organoclay synthesised by using a surfactant molecule with two alkyl chains. This study is of great importance for understanding the structure, properties, and potential applications of these types of organoclays, especially in water purification [1-5, 7, 35, 36].

Experimental:

Materials

Montmorillonite $(Na_{0.053}Ca_{0.176}Mg_{0.1}\bullet nH_2O)[Al_{1.58}Fe_{0.03}Mg_{0.39}][Si_{3.77}Al_{0.23}]O_{10}(OH)_2$ used was primarily Ca-Mt from Neimeng, China. The montmorillonite was cation exchanged with sodium ions by repeated reaction with sodium carbonate. Its cation exchange capacity (CEC) is 90.8meq/100g. The paranitrophenol and DDOAB used were of analytical grade chemical reagents. The aqueous solubility of paranitrophenol is 1.6×10^4 mg/L at 25 °C. The surfactant used was dimethyldioctadecylammonium bromide labeled as DDOAB of formula $(CH_3(CH_2)_{17})_2NBr(CH_3)_2$.

Preparation of the organoclay

The syntheses of surfactant-clay hybrids were undertaken by each of the following procedure: The pure Ca-Mt was added into Na_2CO_3 solution, stirred for 3h with 800rpm. Drops of HCl were then added into the suspension to remove the excess CO_3^{2-}. Then the suspension was washed several times with deionized water until it was chloride free and dried at 108°C. Such a treated montmorillonite is designated as Na-Mt. This procedure is similar to the preparation of $HDTMA^+$ organoclay [37]. The clarifying surfactant solution was obtained when certain amounts DDOAB were added into hot distilled water. Then certain amounts Na-Mt were added into the above mentioned solution and the mixtures were stirred slightly in order to avoid the yield of spume in an 80 °C water bath for 2h. The water/ Na-Mt mass ratio is 10. Then the suspension was subsequently washed with distilled water for 4 times. The moist solid material was dried at 60°C and ground with a mortar. The different amounts of $[DDOA]^+$ pillared montmorillonites were identified by 0.5CEC-D, 0.7CEC- D,

1.5CEC- D, 2.5CEC- D. The figures mean the proportions of the montmorillonite total ion exchange capacity that is $[DDOA]^+$.

Adsorption of the paranitrophenol on the organoclay

A total of 0.2g of different type montmorillonites were combined with 30mL of a range of concentrations of paranitrophenol solution whose initial pH value is about 5.0 in 50mL Erlenmeyer flasks with glass caps. A range of concentrations from 100 mg/L to 8000 mg/L were used for the adsorption of paranitrophenol. The flasks were shaken for 6 hours at 150rpm at 25 °C. After being centrifuged at 3500rpm for 10 minutes, the paranitrophenol concentration in the aqueous phase was determined by a UV-260 spectrophotometer at 317nm, the detection limits being 0.05mg/L. The losses of the paranitrophenol by both photochemical decomposition and volatilization were found to be negligible during adsorption [38].

Characterization methods

Thermogravimetric analysis

Thermogravimetric analyses of the surfactant modified montmorillonite hybrids were obtained using a TA Instruments Inc. Q500 high-resolution TGA operating at ramp 10 °C /min with resolution 6.0 from room temperature to 1000 °C in a high-purity flowing nitrogen atmosphere (60 cm^3/min). Approximately 50 mg of finely ground sample was heated in an open platinum crucible. For the thermogravimetric analyses 4000 mg/L of paranitrophenol was used for the adsorption prior to TG analysis. This concentration was chosen as it is in the mid range of the concentrations used. The samples were identified by 0.5CEC-D-4000, 0.7CEC- D-4000, 1.5CEC- D-4000, 2.5CEC- D-4000.

X-ray diffraction

The Neimeng montmorillonite and surfactant montmorillonite hybrids were pressed in stainless steel sample holders. X-ray diffraction (XRD) patterns were recorded using CuKα radiation (n = 1.5418Å) on a Philips PANalytical X' Pert PRO diffractometer operating at 40 kV and 40 mA with 0.25° divergence slit, 0.5° anti-scattter slit, between 1.5 and 20° (2θ) at a step size of 0.0167°. For XRD at low angle section, it was between 1 and 5° (2θ) at a step size of 0.0167° with variable divergence slit and 0.125° antiscatter. For the XRD analyses 4000 mg/L of paranitrophenol was used for the adsorption on the organoclays prior to powder XRD analysis.

Transmission Electron Microscopy

A Philips CM 200 transmission electron microscopy (TEM) at 200KV is used to investigate the microstructural of organo-clays. All samples were dispersed in 50% ethanol solution and then dropped on carbon coated films, dried in an oven at 50°C for 10 mins for TEM studies without using any resin.

Infrared spectroscopy

Infrared spectra were obtained using a Nicolet Nexus 870 FTIR spectrometer with a smart endurance single bounce diamond ATR cell. Spectra over the 4000–550 cm^{-1} range were obtained by the co-addition of 64 scans with a resolution of 4 cm^{-1} and a mirror velocity of 0.6329 cm/s. Spectral manipulation such as baseline adjustment, smoothing and normalization was performed using the GRAMS® software package (Galactic Industries Corporation, Salem, NH, USA).

Infrared emission spectroscopy

FTIR emission spectroscopy was carried out on a Nicolet Nexus 870 FTIR spectrometer, which was modified by replacing the IR source with an emission cell. A description of the cell and principles of the emission experiment have been published elsewhere . Approximately 0.2 mg of the sample was spread as a thin layer on a 6 mm diameter platinum surface and held in an inert atmosphere within a nitrogen-purged cell during heating. The infrared emission cell consists of a modified atomic absorption graphite rod furnace, which is driven by a thyristor-controlled AC power supply capable of delivering up to 150 amps at 12 volts. A platinum disk acts as a hot plate to heat the sample and is placed on the graphite rod. An insulated 125-μm type R thermocouple was embedded inside the platinum plate in such a way that the thermocouple junction was <0.2 mm below the surface of the platinum. Temperature control of ± 2°C at the operating temperature of the sample was achieved by using a Eurotherm Model 808 proportional temperature controller, coupled to the thermocouple.

The design of the IES facility is based on an off axis paraboloidal mirror with a focal length of 25 mm mounted above the heater captures the infrared radiation and directs the radiation into the spectrometer. The assembly of the heating block, and platinum hot plate is located such that the surface of the platinum is slightly above the focal point of the off axis paraboloidal mirror. By this means the geometry is such that approximately 3 mm diameter area is sampled by the spectrometer. The spectrometer was modified by the removal of the source assembly and mounting a gold coated mirror, which was drilled through the centre to allow the passage of the laser beam. The mirror was mounted at 45°, which enables the IR radiation to be directed into the FTIR spectrometer.

In the normal course of events, three sets of spectra are obtained: firstly the black body radiation over the temperature range selected at the various temperatures, secondly the platinum plate radiation is obtained at the same temperatures and thirdly the spectra from the platinum plate covered with the sample. Normally only one set of black body and platinum radiation is required. The emittance spectrum at a particular temperature was calculated by subtraction of the single beam spectrum of the platinum backplate from that of the platinum + sample, and the result ratioed to the single beam spectrum of an approximate blackbody (graphite). This spectral manipulation is carried out after all the spectral data has been collected.

The emission spectra were collected at intervals of 50°C over the range 100 – 700 °C. The time between scans (while the temperature was raised to the next hold

point) was approximately 100 seconds. It was considered that this was sufficient time for the heating block and the powdered sample to reach temperature equilibrium. The spectra were acquired by coaddition of 64 scans for the whole temperature range (approximate scanning time 45 seconds), with a nominal resolution of 4 cm^{-1}. The number of scans varied with the sample and temperature and was selected to give high quality spectra and varied from 64 to 1024. Good quality spectra can be obtained providing the sample thickness is not too large. Spectral manipulation such as baseline adjustment, smoothing and normalisation was performed using the Spectracalc software package (Galactic Industries Corporation, NH, USA).

Results and Discussion

X-ray diffraction

Expansion of the montmorillonite layers occurs with the cation exchange of the sodium ion for the cationic surfactant and is easily measured by X-ray diffraction.

The powder XRD patterns of the Na montmorillonite and the organoclays with 0.5, 1.5 and 2.5 CEC surfactant concentrations with and without adsorbed paranitrophenol are shown in Figure 1. The Na montmorillonite originally with a d(001) spacing of 1.24 nm expands after ion exchange with DDOAB at the 0.5CEC level, to 1.46, 1.94 and 3.35 nm. The reason for the three spacings is attributed to the arrangement of the DDOAB surfactant molecule in the clay layers. The d(001) spacing of 1.46 nm is a similar space to the Na montmorillonite. This spacing is attributed to Na-Mt. Upon adsorption of the paranitrophenol on the montmorillonite (Na-4000) a small expansion of the clay layers from 1.24 nm to 1.49 nm is observed. This increase proves that the paranitrophenol penetrated the siloxane layers. The spacing of 1.94 nm is ascribed to the montmorillonite expanded with the surfactant molecule with the molecule lying parallel to the siloxane surfaces (0.5CEC-D). The 3.35 nm spacing is attributed to the surfactant molecules at right angles to the clay surface (0.5CEC-D). Upon adsorption of paranitrophenol on the organoclay surfaces structural rearrangement of the surfactant molecules between the clay layers occurs (0.5CEC-D-4000). For the 0.5 CEC organoclay with adsorbed paranitrophenol, two expansions of 1.47 and 1.83 nm were found. No large expansion as for the 0.5CEC-D organoclay was found. These values suggest that the pnp has penetrated the clay layers and has bonded to the surfactant molecule within the clay layers.

When the surfactant loading is increased to 1.5 CEC, three d(001) spacings are observed at 1.18 nm attributed to Na-Mt, 1.80 nm assigned to a molecular arrangement with the surfactant molecules laying flat to the surface and 3.59 nm attributed to the surfactant molecules at 90° to the siloxane surface. Upon increasing the surfactant loading to 2.5 CEC, d(001) spacings of 1.93 and 4.96 nm are observed. This latter large d(001) spacing is described in terms of overlapping surfactant molecules in a paraffin-like arrangement between the clay layers. For the 1.5 CEC organoclay with adsorbed paranitrophenol, spacings of 1.0, 1.34, 1.99 and 3.91 nm are observed. The 1.00 nm spacing is ascribed to montmorillonite with a collapsed structure in which the surfactant molecule has not been intercalated and has not been replaced with water. The 1.34 nm spacing is ascribed to the organoclay with minimal paranitrophenol adsorption. The 1.99 and 3.91 nm expanded layers is attributed to

surfactant molecules with adsorbed pnp between the clay layers. These two expansions may be compared with the 1.8 and 3.59 nm expansions of the 1.5 CEC organoclay without adsorbed paranitrophenol. The difference in the values (3.91-3.59 nm) and (1.99-1.80 nm) is attributed to the size of the paranitrophenol molecule. This proves that the paranitrophenol is intercalated into the montmorillonite clay and is part of the molecular arrangement within the clay interlayer. Similar values were obtained for the 2.5 CEC organoclay with adsorbed paranitrophenol. Here expansions of 1.00, 1.33, 1.98 and 3.81 nm are observed. It is proposed that these results prove that the paranitrophenol molecules are intercalated into the clay layers.

TEM

Often the results of the powder X-ray diffraction basal spacings can be confirmed by the use of TEM measurements. The TEM images of 1.5CEC-D and 1.5CEC-D-4000 organoclay are shown in Figure 2. Two spacings for the 1.5CEC-D organoclay are observed at 1.17 and 1.85 nm. These spacings are in good agreement with the XRD data. For the 1.5 CEC-D-4000 organoclay spacings are observed at 1.02, 1.36, 2.0 and 3.96 nm. In the XRD patterns for the 1.5CEC-D-4000 d(001) spacings at 1.0, 1.34, 1.99 and 3.91 nm. The correspondence between the XRD results and the TEM data is excellent. The d(001) spacings for the 2.5 CEC organoclay with adsorbed pnp as illustrated in are 1.37 and 1.98 nm (not shown). These values correspond to the d(001) spacings in the XRD patterns of 1.33 and 1.98 nm. Two spacings are observed in the TEM image of the 2.5CEC-D-4000 organoclay at 0.95 and 3.8 nm. These correspond to the d(001) spacings of 1.0 and 3.81 nm.

Thermogravimetric analysis

The TG and DTG patterns of the paranitrophenol and the surfactant molecule DDOAB are shown in Figure 3. Paranitrophenol sublimes at 131 °C with a total mass loss of 99.20 %. The DDOAB shows thermal decomposition steps at 166, 244 and 304 °C attributed to decomposition/combustion of the surfactant molecules with a mass loss of 99.77 %. This value is a good indication of the purity of the surfactant.

The TG/DTG patterns for Na-Mt, Na-Mt-4000, 0.5CEC-D, 0.5CEC-D-4000, 1.5CEC-D and 1.5CEC-D-4000 are shown in Figure 4. The montmorillonite shows thermal decomposition steps at 485 and 617 °C. These are attributed to the dehydroxylation of the montmorillonite. The DTG patterns for Na-Mt-4000 shows decomposition steps at 179, 285, 625 and 797 °C. The first DTG step at 179 °C is assigned to the sublimation of surface adsorbed pnp, the second step at 285 °C is to intercalated pnp, the third step at 625 °C is attributed to the clay dehydroxylation. The higher temperature decomposition at 797 °C may be attributed to the dehydroxylation of the montmorillonite where no simple mechanism of dehydroxylation is available for this process and so an increased temperature is observed.

The 0.5 CEC-D differential thermogravimetric pattern shows peaks at 300, 389 and 590 °C. A slight decrease in the dehydroxylation of the clay is observed (590 compared with 617 °C). The peaks at 389 and 300 °C are higher than is observed for the surfactant. This suggests that the surfactant molecule is bonded to the clay surfaces and more heat is required to remove the surfactant molecules from the clay

surfaces. The DTG pattern for the 0.5 CEC-D-4000 (organoclay with adsorbed pnp) is quite different to that of the 0.5 CEC organoclay. Three decomposition temperatures are observed at 189, 286, and 382°C. A higher temperature decomposition at 544 °C is observed. Interestingly the dehydroxylation temperature of 590 °C for the clay is not observed. This suggests the reaction of the clay siloxane surfaces with pnp occurs through the OH units of the montmorillonite and the dehydroxylation temperature is reduced to 544 °C. The temperature of 382 °C represents the combustion of the surfactant. The two peaks at 286 and 189 °C are attributed to the combustion of the surfactant and as no DTG peaks attributable to the pnp are observed, it is proposed that the pnp is removed simultaneously with the surfactant.

The thermal decomposition steps for the 0.7 CEC organoclay (not shown) are similar to that for the 0.5 CEC organoclay with DTG peaks observed at 293, 396 and 590 °C. The latter is due to the montmorillonite and the first two steps to the loss of the surfactant. For the 0.7 CEC organoclay with adsorbed pnp, DTG peaks are observed at 193, 283 and 385 °C. No peak is found at 590 °C. This suggests that the pnp results in the lowering of the clay dehydroxylation temperature. For the 1.5CEC-D, DTG peaks are observed at 229, 341, 392 and 590 °C (Figure 4). The first three peaks are ascribed to the combustion of the surfactant and the latter to the dehydroxylation of the montmorillonite. It is noted that the three temperatures (229, 341, 392 °C) are significantly higher than for the DTG peaks of the surfactant (166, 244, and 304 °C. This difference in temperatures is attributed to the bonding of the surfactant molecules to the montmorillonite surfaces. Heating the organoclay to higher temperatures is required before the surfactant molecules are removed. Thermal decomposition of 1.5CEC-D-4000 shows thermal decomposition steps at 195, 232, 288, 328 and 409 °C. The first step is attributed to the loss of surface adsorbed pnp, the second to the loss of intercalated pnp, the third and fourth steps to the loss of surfactant. The last step is probably the dehydroxylation of the montmorillonite. Thermal decomposition peaks are observed at 178, 241, 295, 346 and 600 °C for the 2.5CEC-D organoclay. The first three peaks correspond to the three thermal decomposition steps of DDOAB at 166, 244 and 304 °C and are attributed to the loss of surfactant molecules. This temperature correspondence indicates that at 2.5CEC the surfactant molecules are not only intercalated within the montmorillonite layers but also are adsorbed on the external surfaces of the clay. The temperature of dehydroxylation of the montmorillonite is now observed at 600 °C. For the 2.5CEC-D-4000, thermal decomposition steps are observed at 180, 231, 285, 336 and 412 °C. The first three decomposition steps are assigned to the loss of surfactant. The decomposition steps at 336 and 412 are attributed to the loss of intercalated surfactant molecules and the dehydroxylation of the montmorillonite. It is assumed that the loss of the pnp occurs simultaneously with the surfactant.

Infrared emission spectroscopy

OH stretching region

The infrared emission spectra in the OH stretching region of (a) montmorillonite with adsorbed paranitrophenol (b) 0.5CEC-D-4000 (c) 1.5CEC-D-4000 (d) 2.5CEC-D-4000 are shown in Figures 5a-d.

The infrared spectrum of Na-Mt at room temperature displays a band at 3612 cm^{-1} attributed to the inner hydroxyl units within the clay structure. Bands at 3394 and 3235 are attributed to adsorbed water. The less intense band observed at 3235 cm^{-1} is ascribed to water hydrogen bonded to other water molecules within the interlayer of the montmorillonite. These molecules are involved with the structure of the hydration sphere of the cation within the montmorillonite interlayer. The infrared spectrum sodium montmorillonite with adsorbed paranitrophenol shows peaks in similar positions to that of montmorillonite (Figure 5a). Infrared bands are observed in the IE spectra at 3623 and 3521 cm^{-1} and shift to 3650 and 3529 cm^{-1} with an additional band at 3735 cm^{-1} observed in the higher temperature spectra. The infrared spectrum of the paranitrophenol displays peaks at 3400 and 3318 cm^{-1}. These bands are assigned to OH stretching vibrations of the phenol unit. The first band is assigned to non-hydrogen bonded phenol OH units and the second to hydrogen bonded OH units. The intensity of this second band is greater than that of the first band. Two types of hydrogen bonding are possible (a) hydrogen bonding of pnp with itself and (b) hydrogen bonding of the pnp with water. This latter bonding is proposed as a mechanism for the adsorption of pnp on montmorillonite. No bands for paranitrophenol are observed in this spectral region.

The IE spectra of 0.5CEC-D-4000 are shown in Figure 5b. No bands ascribed to either the surfactant molecules or the paranitrophenol are observed in this spectral region. All of the labeled bands are due to hydroxyl units of the Na-Mt. The band at 3625 cm^{-1} is attributed to the inner hydroxyl units. The band shifts to higher wavenumbers with thermal treatment. A second band is found at 3681 cm^{-1} and may be ascribed to sheet end hydroxyl units. This band is not observed at higher temperatures indicating these OH units are more easily lost. An additional band is observed at 3521 cm^{-1}. This band is not observed at all in the 1.5CEC-D-4000 spectrum. The two bands at 3617 and 3662 cm^{-1} are now more clearly resolved. The latter band shifts to 3689 cm^{-1} at 450 °C. This band appears to be related to the influence of the surfactant molecules and one possible assignment is to OH units which are interacting with the surfactant molecules. A similar set of spectra are observed for the 2.5CEC-D-4000 spectra.

CH stretching region

The IE spectra of the Na-4000 clay are shown in Figure 6a. Two bands are observed at 2856 and 2929 cm^{-1} attributed to the symmetric and antisymmetric CH stretching vibrations of the paranitrophenol. These bands are lost by 300 °C. This temperature corresponds to the sublimation of the paranitrophenol. Some low intensity bands are observed at 2223 and 2350 cm^{-1}. These are ascribed to overtone bands. No bands which are due to the clay are observed in this spectral region. For the 0.5CEC-D-4000 strong IE bands are observed at 2858 and 2931 cm^{-1}. Intensity in these bands is quite strong up to 450 °C. At higher temperatures the surfactant is lost through combustion. A similar set of spectra is observed for 1.5CEC-D-4000 and 2.5CEC-D-4000. The peak at 2350 cm^{-1} is due to self absorption probably by atmospheric carbon dioxide.

HCH and HOH bending vibrations

The IE spectra of Na-4000 are displayed in Figure 7a. Bands in this spectral

region can only be attributed to pnp vibrations or to the montmorillonite. Pnp infrared spectrum shows a number of bands at 1623 assigned to HOH deformation modes;1599 ascribed to C=C aromatic stretching vibrations, 1523 attributed to antisymmetric NO_2 stretching vibrations; 1485 described as C-H in-plane bending vibrations; 1332 and 1296 cm^{-1} described by symmetric NO_2 stretching vibrations + C-O stretching vibrations [39]. When the pnp is adsorbed on the montmorillonite shifts in the position of the bands are observed. The band at 1599 shifts to 1593 cm^{-1}; 1523 shifts to 1510 cm^{-1}; 1332 to 1340 cm^{-1}; 1296 to 1281 cm^{-1}. The shifts in these bands provide strong indication that the pnp has reacted with the montmorillonite clay surfaces. The band at 1629 cm^{-1} is assigned to water bending modes of the water in the hydration sphere within the clay interlayer. The intensity of this band decreases with surfactant loading. The band also shifts to higher wavenumber (~1640 cm^{-1}) in the organoclays. It is noted that the intensity of the bands attributed to paranitrophenol decrease in intensity until a temperature of 400 °C. This temperature is significantly higher than the temperature of sublimation of paranitrophenol at 131 °C. This provides evidence for the bonding of the paranitrophenol to the surface of the montmorillonite surfaces. It is suggested that the paranitrophenol molecule interacts with the inner OH units of the montmorillonite and possibly forms a chemical bond. This then results in the retention of the paranitrophenol molecules to quite elevated temperatures and also provides a mechanism for the dehydroxylation of the montmorillonite inner OH units. This results in a significant decrease in the dehydroxylation temperatures

The IE spectra of the 0.5CEC-S-4000 organoclay with adsorbed pnp are shown in Figure 7b. Any additional peaks over and above those shown in Figure 5a must be attributed to the surfactant molecules. Thus bands at 1593, 1516, 1467, 1384, 1336 and 1292 cm^{-1} may be at least in part attributed to vibrations of the DDOAB surfactant molecules. Importantly the band at 1467 cm^{-1} is retained at 400 °C, thus giving an indication of the retention of the surfactant at this temperature. The implication is that the organoclay is stable up to 400 °C. Such a concept is confirmed by the IE spectra of the 1.5CEC-S-4000 and 1.5CEC-S-4000 samples (Figure 7c,d). The ~1462 cm^{-1} band is retained up to 400 °C.

SiO stretching bands

The IE spectra of the Na-4000 sample are shown in Figure 8a. The infrared spectrum of paranitrophenol shows a number of strong absorptions at 1178, 1122, 850, 754 and 625 cm^{-1}. The first two bands are attributed to C-H in-plane bending vibrations. The band at 754 cm^{-1} is assigned to the NO_2 wagging vibration. Small shifts in these band positions are observed when the pnp is adsorbed on the montmorillonite (Figure 8b). The 1178 cm^{-1} band shifts to 1170; 1122 to 1111 cm^{-1}; ~ 852 cm^{-1}; 754 to 756 cm^{-1} and 625 to 669 cm^{-1}. The intensity in these bands is lost by 300 °C indicating the pnp molecules have sublimed by this temperature. The broad bands which remain after this sublimation are attributed to SiO stretching and bending vibrations. For the 1.5CEC-D-4000 infrared bands are observed as shown in Figure 8c. A significant number of bands which may be attributed to the surfactant molecules are observed at 1163, 1134, 1102 cm^{-1} the intensity of which is lost by 300 °C. The infrared emission spectra of the 2.5CEC-D-4000 infrared bands are observed as shown in Figure 8d.

Conclusions:

The current study of sorption of paranitrophenol from aqueous solutions provides useful application of montmorillonite and a series of organoclays. The surfactant molecules are retained on the clay surfaces up to 400 °C significantly above the temperature of combustion of the surfactant molecules which is evidenced by IES data. The paranitrophenol is adsorbed on the mentioned sorbents and the sorption of paranitrophenol results in the rearrangement of the interlayer surfactant and the lowering of the dehydroxylation temperature of the montmorillonite which is evidenced by X-ray diffraction and TEM and TG. The thermogravimetric data indicate the behavior of the organic compounds which included the paranitrophenol and surfactant (DDOAB).

This work has shown that

a) Paranitrophenol is adsorbed and is probably chemically bonded to the montmorillonite.
b) The paranitrophenol is not lost until temperatures significantly above the normal sublimation temperature of paranitrophenol
c) The surfactant DDOAB of formula $(CH_3(CH_2)_{17})_2NBr(CH_3)_2$. is bonded to the siloxane surfaces of the montmorillonite.
d) The surfactant molecules are retained on the clay surfaces up to 400 °C significantly above the temperature of combustion/decomposition of the DDOAB surfactant molecules.
e) The adsorption of paranitrophenol is greater on the DDOAB organoclay than the Na-montmorillonite
f) The adsorption of the paranitrophenol depends upon the CEC concentration and consequently upon the arrangement of the surfactant molecules in the clay interlayer
g) The adsorption of the paranitrophenol results in the lowering of the dehydroxylation temperature of the montmorillonite
h) The organoclays based upon DDOAB are stable up to ~400 °C

Acknowledgements

This work was funded by National Natural Science Foundation of China (Grant No. 40372029) and Natural Science Foundation of Guangdong Province (Grant No. 030471 and 05103410). The Inorganic Materials Research Program, Queensland University of Technology, is gratefully acknowledged for infra-structural support.

References

1. Abate, G., Dos Santos, L. B. O., Colombo, S. M. and Masini, J. C., *Applied Clay Science* 32, 261 (2006).
2. Akcay, G. and Yurdakoc, K., *Acta Hydrochimica et Hydrobiologica* 28, 300 (2000).
3. Alther, G., *Contaminated Soils* 7, 223 (2002).
4. Alther, G. R., *Journal - American Water Works Association* 94, 115 (2002).
5. Beall, G. W., *Applied Clay Science* 24, 11 (2003).
6. Chun, Y., Sheng, G. and Boyd, S. A., *Clays and Clay Minerals* 51, 415 (2003).
7. Groisman, L., Rav-Acha, C., Gerstl, Z. and Mingelgrin, U., *Applied Clay Science* 24, 159 (2004).
8. Rytwo, G. and Gonen, Y., *Colloid and Polymer Science* 284, 817 (2006).
9. Zhang, X.-K., Zhang, W.-Q. and Zou, H.-X., *Nongye Huanjing Kexue Xuebao* 23, 400 (2004).
10. Zhu, L., Pan, Q., Chen, S., Zhang, J. and Wei, L., *Shuichuli Jishu* 22, 107 (1996).
11. Zhao, H. and Vance, G. F., *Water Research* 32, 3710 (1998).
12. Yariv, S., *Thermochimica Acta* 274, 1 (1996).
13. Taylor, R. S., Davies, M. E. and Williams, J., in *PCT Int. Appl.*, (Laporte Industries Ltd., UK). Wo, 1992, p. 16 pp.
14. Wang, X., Wu, S., Li, W. and Sheng, G., *Huanjing Huaxue* 16, 1 (1997).
15. Sutton, P. A., *Proceedings of the Annual Meeting Technical Program of the FSCT* 78th, 637 (2000).
16. Sand, I. D., Piner, R. L., Gilmer, J. W. and Owens, J. T., in *U.S.*, (Eastman Chemical Company, USA). Us, 2003, p. 8 pp.
17. Rafailovich, M., Si, M. and Goldman, M., in *PCT Int. Appl.*, (The Research Foundation of State University of New York, USA). Wo, 2003, p. 34 pp.
18. Pinnavaia, T. J., Lan, T., Wang, Z., Shi, H. and Kaviratna, P. D., *ACS Symposium Series* 622, 250 (1996).
19. Xi, Y., Ding, Z., He, H. and Frost, R. L., *Spectrochimica Acta, Part A: Molecular and Biomolecular Spectroscopy* 61A, 515 (2005).
20. He, H., Yang, D., Yuan, P., Shen, W. and Frost Ray, L., *Journal of colloid and interface science* 297, 235 (2006).
21. He, H., Frost, R. L., Bostrom, T., Yuan, P., Duong, L., Yang, D., Xi, Y. and Kloprogge, J. T., *Applied Clay Science* 31, 262 (2006).
22. He, H. P., Ding, Z., Zhu, J. X., Yuan, P., Xi, Y. F., Yang, D. and Frost, L. R., *Clays and Clay Minerals* 53, 287 (2005).
23. Xi, Y., Ding, Z., He, H. and Frost, R. L., *Journal of Colloid and Interface Science* 277, 116 (2004).
24. Xi, Y., Frost, R. L., He, H., Kloprogge, T. and Bostrom, T., *Langmuir* 21, 8675 (2005).
25. Xi, Y., Frost Ray, L., He, H., Kloprogge, T. and Bostrom, T., *Langmuir : the ACS journal of surfaces and colloids* 21, 8675 (2005).
26. Xi, Y., Martens, W., He, H. and Frost, R. L., *Journal of Thermal Analysis and Calorimetry* 81, 91 (2005).
27. Xi, Y., Ding, Z., He, H. and Frost Ray, L., *Journal of colloid and interface science* 277, 116 (2004).
28. Boyd, S. A., Shaobai, S., Lee, J.-F. and Mortland, M. M., *Clays and Clay Minerals* 36, 125 (1988).

29. Mortland, M. M., Shaobai, S. and Boyd, S. A., *Clays and Clay Minerals* 34, 581 (1986).
30. Smith, J. A., Jaffe, P. R. and Chiou, C. T., *Environmental Science and Technology* 24, 1167 (1990).
31. Wang, P., (Peop. Rep. China). Application: CN
CN, 2006, p. 9pp.
32. Kim, J.-H., Shin, W. S., Song, D.-I. and Choi, S. J., *Korean Journal of Chemical Engineering* 23, 63 (2006).
33. Gonen, Y. and Rytwo, G., *Journal of Colloid and Interface Science* 299, 95 (2006).
34. Zhou, Q., He, H. P., F., X. Y. and Frost, R. L., *J. Colloid Interf. Sci.* (2006).
35. Alther, G. R., *Oils and Environment, Proceedings of [the] International Conference, 4th, Gdansk, Poland, June 20-23, 2005* 434 (2005).
36. Oyanedel-Craver, V. A. and Smith, J. A., *Journal of Hazardous Materials* 137, 1102 (2006).
37. He, H. P., Zhou, Q., Wayde, N. M., Kloprogge, T. J., Yuan, P., F., X. Y., Zhu, J. X. and Frost, R. L., *Clays Clay Miner.* 54, 691 (2006).
38. Zhu, L. and Chen, B., *Environmental Science and Technology* 34, 2997 (2000).
39. Abkowicz-Bienko, A. J., Latajka, Z., Bienko, D. C. and Michalska, D., *Chemical Physics* 250, 123 (1999).

List of Figures

Figure 1 XRD patterns of Na-Mt, Na-Mt-4000, 0.5CEC-D, 0.5CEC-D-4000, 0.7CEC-D, 0.7CEC-D-4000, 1.5CEC-D, 1.5CEC-D-4000, 2.5CEC-D and 2.5CEC-D-4000

Figure 2 Illustrative TEM images of 1.5CEC-D, 1.5CEC-D-4000

Figure 3 Thermogravimetric analysis of paranitrophenol and surfactant DDOAB

Figure 4 Thermogravimetric analysis of Na-Mt, Na-Mt-4000, 0.5CEC-D, 0.5CEC-D-4000, 1.5CEC-D and 1.5CEC-D-4000

Figure 5a Infrared emission spectroscopy of Na-Mt with adsorbed paranitrophenol in the 3000 to 4000 cm^{-1} region.

Figure 5b Infrared emission spectroscopy of 0.5CEC-D-4000 with adsorbed paranitrophenol in the 3000 to 4000 cm^{-1} region.

Figure 5c Infrared emission spectroscopy of 1.5CEC-D-4000 with adsorbed paranitrophenol in the 3000 to 4000 cm^{-1} region.

Figure 5d Infrared emission spectroscopy of 2.5CEC-D-4000 with adsorbed paranitrophenol in the 3000 to 4000 cm^{-1} region.

Figure 6a Infrared emission spectroscopy of Na-Mt with adsorbed paranitrophenol in the 2000 to 3000 cm^{-1} region.

Figure 6b Infrared emission spectroscopy of 0.5CEC-D-4000 with adsorbed paranitrophenol in the 2000 to 3000 cm^{-1} region.

Figure 6c Infrared emission spectroscopy of 1.5CEC-D-4000 with adsorbed paranitrophenol in the 2000 to 3000 cm^{-1} region.

Figure 6d Infrared emission spectroscopy of 2.5CEC-D-4000 with adsorbed paranitrophenol in the 2000 to 3000 cm^{-1} region.

Figure 7a Infrared emission spectroscopy of Na-Mt with adsorbed paranitrophenol in the 1200 to 2000 cm^{-1} region.

Figure 7b Infrared emission spectroscopy of 0.5CEC-D-4000 with adsorbed paranitrophenol in the 1200 to 2000 cm^{-1} region.

Figure 7c Infrared emission spectroscopy of 1.5CEC-D-4000 with adsorbed paranitrophenol in the 1200 to 2000 cm^{-1} region.

Figure 7d Infrared emission spectroscopy of 2.5CEC-D-4000 with adsorbed paranitrophenol in the 1200 to 2000 cm^{-1} region.

Figure 8a Infrared emission spectroscopy of Na-Mt with adsorbed paranitrophenol in the 650 to 1200 cm^{-1} region.

Figure 8b Infrared emission spectroscopy of 0.5CEC-D-4000 with adsorbed paranitrophenol in the 650 to 1200 cm^{-1} region.

Figure 8c Infrared emission spectroscopy of 1.5CEC-D-4000 with adsorbed paranitrophenol in the 650 to 1200 cm^{-1} region.

Figure 8d Infrared emission spectroscopy of 2.5CEC-D-4000 with adsorbed paranitrophenol in the 650 to 1200 cm^{-1} region

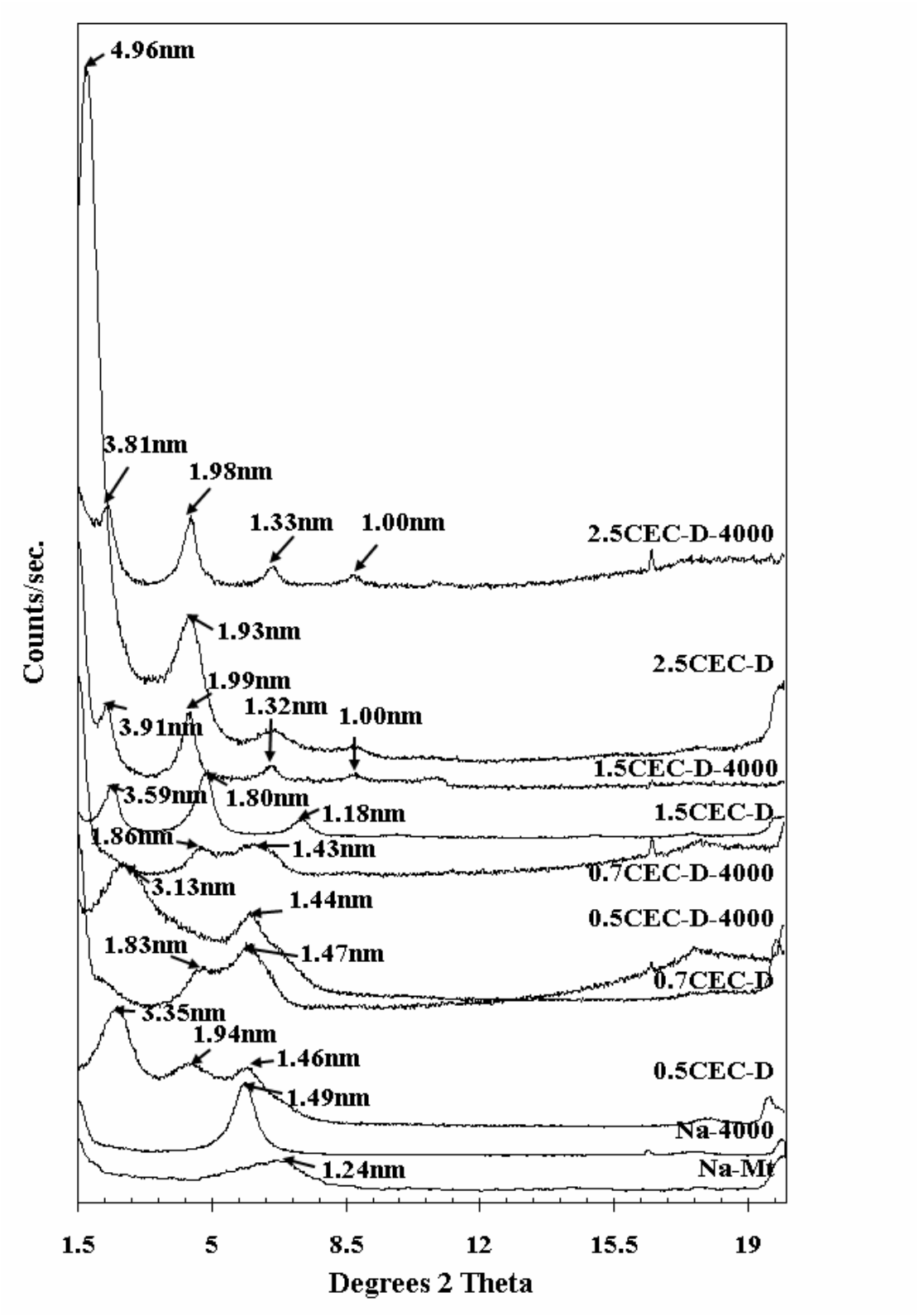
4.96nm
3.81nm
1.98nm
1.33nm
1.00nm
2.5CEC-D-4000
1.93nm
2.5CEC-D
1.99nm
1.32nm
1.00nm
3.91nm
1.5CEC-D-4000
3.59nm
1.80nm
1.18nm
1.5CEC-D-
1.86nm
1.43nm
0.7CEC-D-4000
3.13nm
1.44nm
0.5CEC-D-4000
1.83nm
1.47nm
0.7CEC-D
3.35nm
1.94nm
1.46nm
0.5CEC-D
1.49nm
Na-4000
1.24nm
Na-Mt
Counts/sec.
1.5
5
8.5
12
15.5
19
Degrees 2 Theta

Figure 1

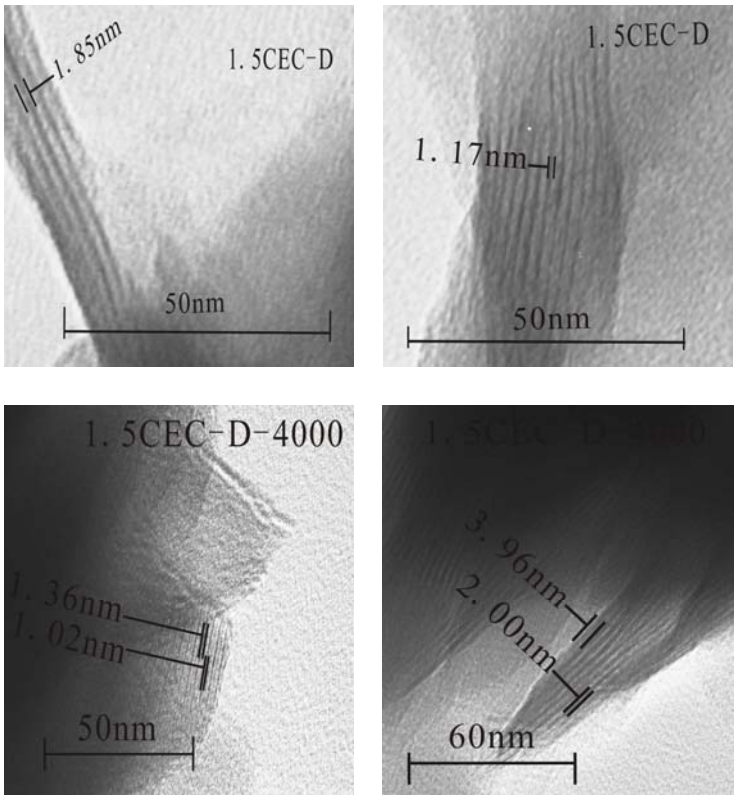
1.85nm
1.5CEC-D
50nm
1.5CEC-D
1.17nm
50nm
1.5CEC-D-4000
1.36nm
1.02nm
50nm
3.96nm
2.00nm
60nm

Figure 2

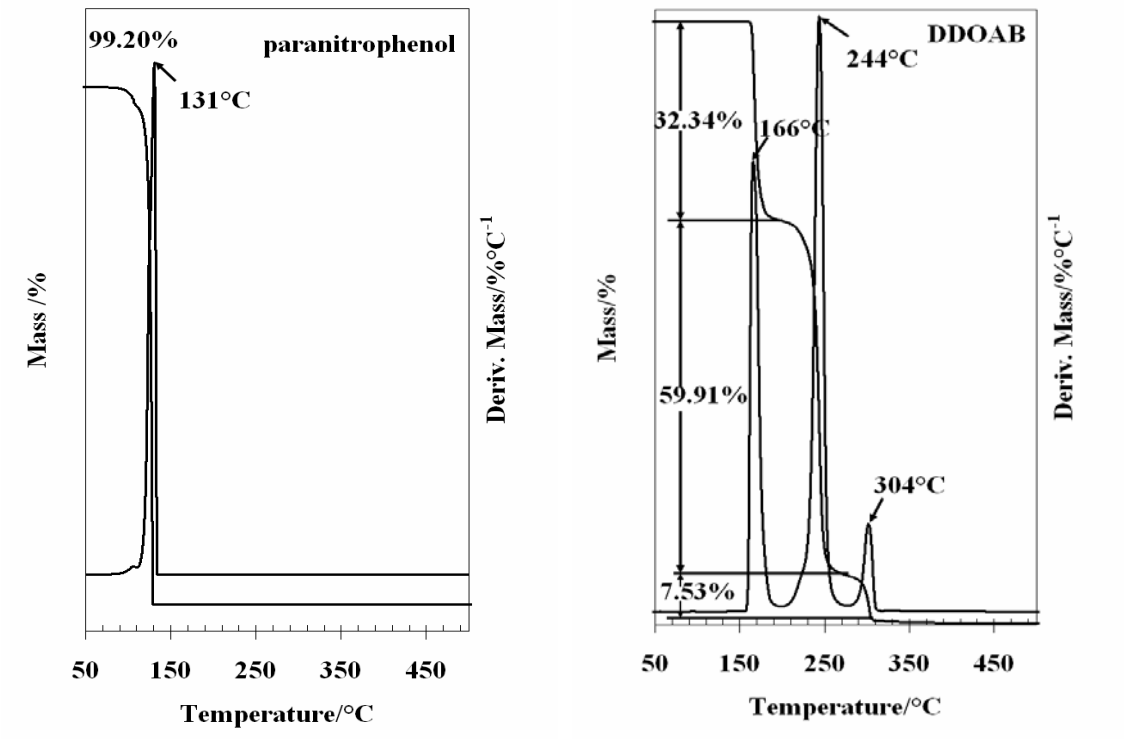
99.20%
paranitrophenol
131°C
Mass /%
Deriv. Mass/%°C-1
50
150
250
350
450
Temperature/°C
DDOAB
244°C
32.34%
166°C
Mass/%
59.91%
304°C
7.53%
Deriv. Mass/%°C-1
50
150
250
350
450
Temperature/°C

Figure 3

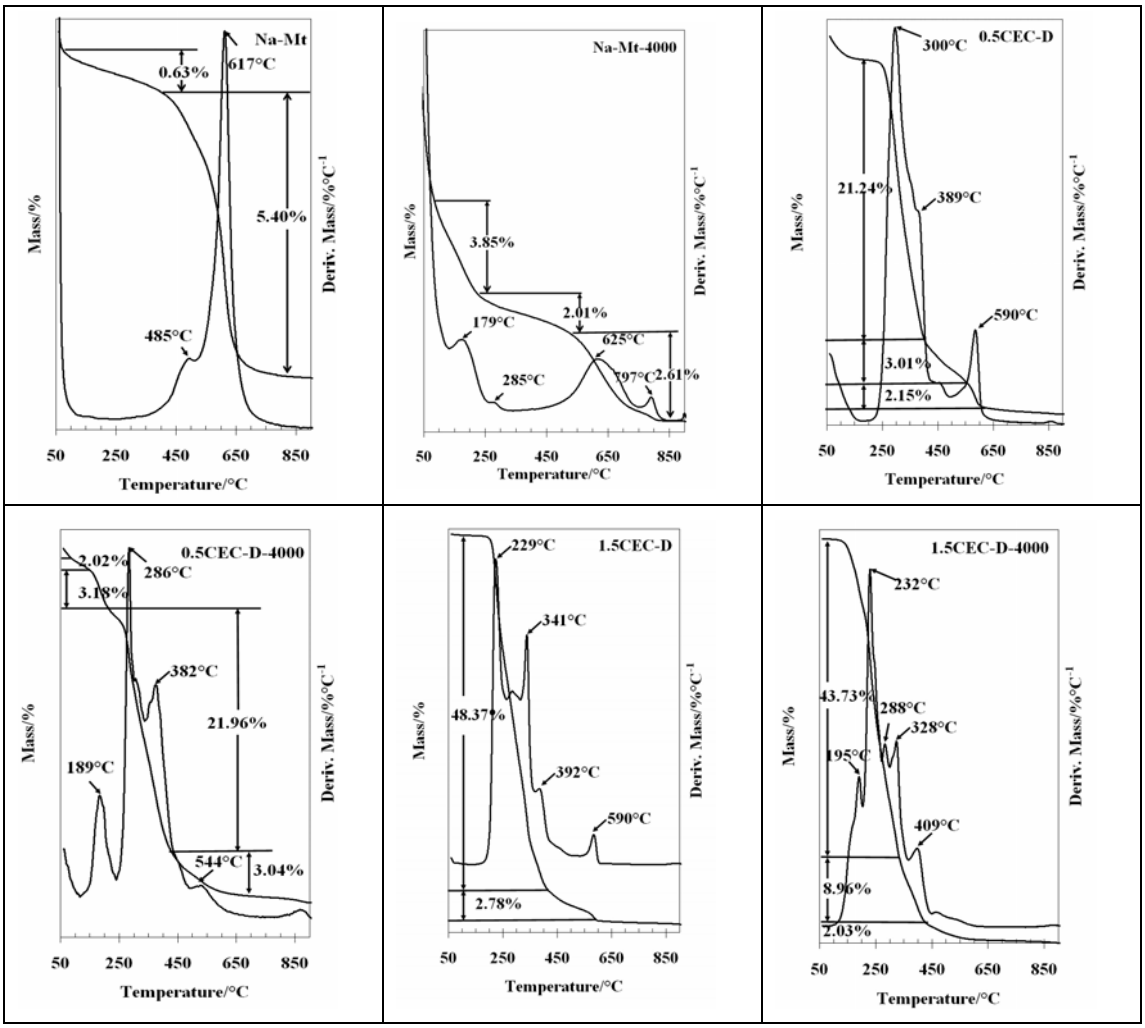
Na-Mt
0.63%
617°C
5.40%
485°C
Mass/%
Deriv. Mass/%°C-1
50 250 450 650 850
Temperature/°C
Na-Mt-4000
3.85%
2.01%
179°C
625°C
285°C
597°C
2.61%
0.5CEC-D
300°C
21.24%
389°C
590°C
3.01%
2.15%
0.5CEC-D-4000
2.02%
286°C
3.18%
382°C
21.96%
189°C
544°C
3.04%
1.5CEC-D
229°C
341°C
48.37%
392°C
590°C
2.78%
1.5CEC-D-4000
232°C
43.73%
288°C
328°C
195°C
409°C
8.96%
2.03%

Figure 4

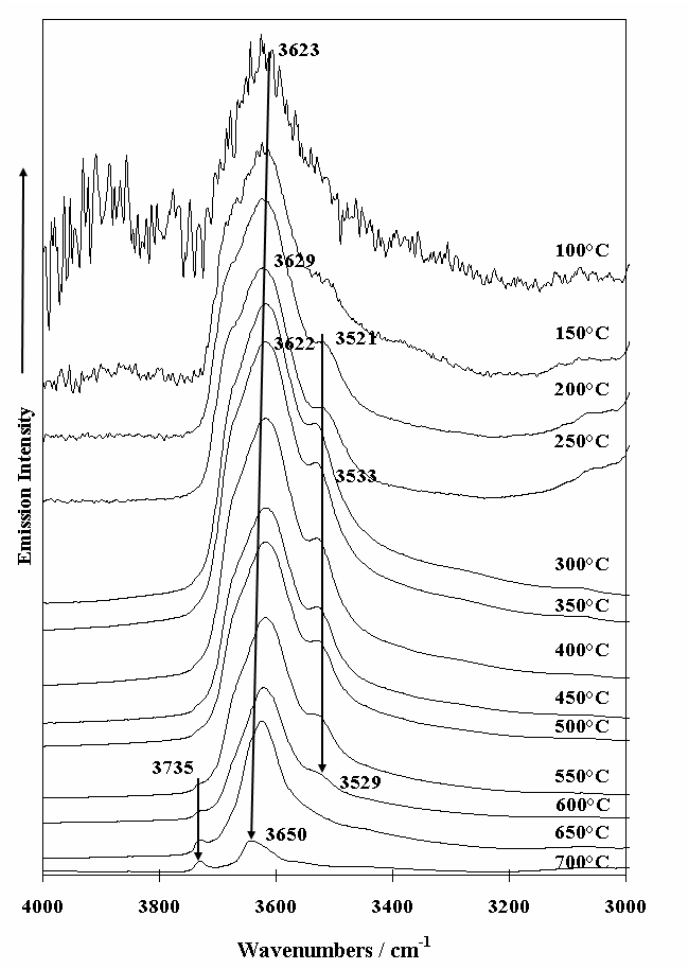

Figure 5a Montmorillonite with adsorbed pnp

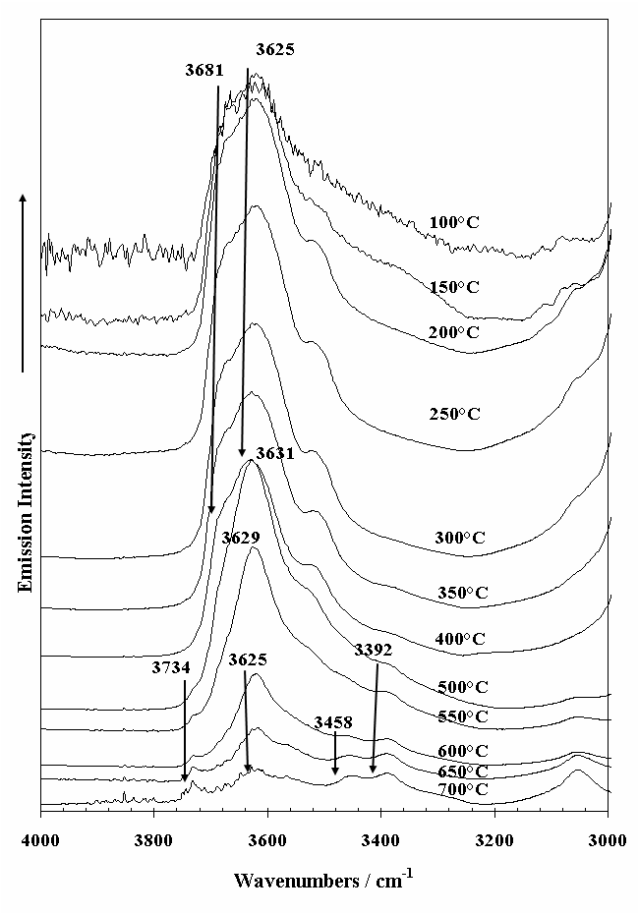
3625
3681
100°C
150°C
200°C
250°C
3631
300°C
3629
350°C
400°C
3734
3625
3392
500°C
550°C
3458
600°C
650°C
700°C
Emission Intensity
4000
3800
3600
3400
3200
3000
Wavenumbers / cm-1

Figure 5b

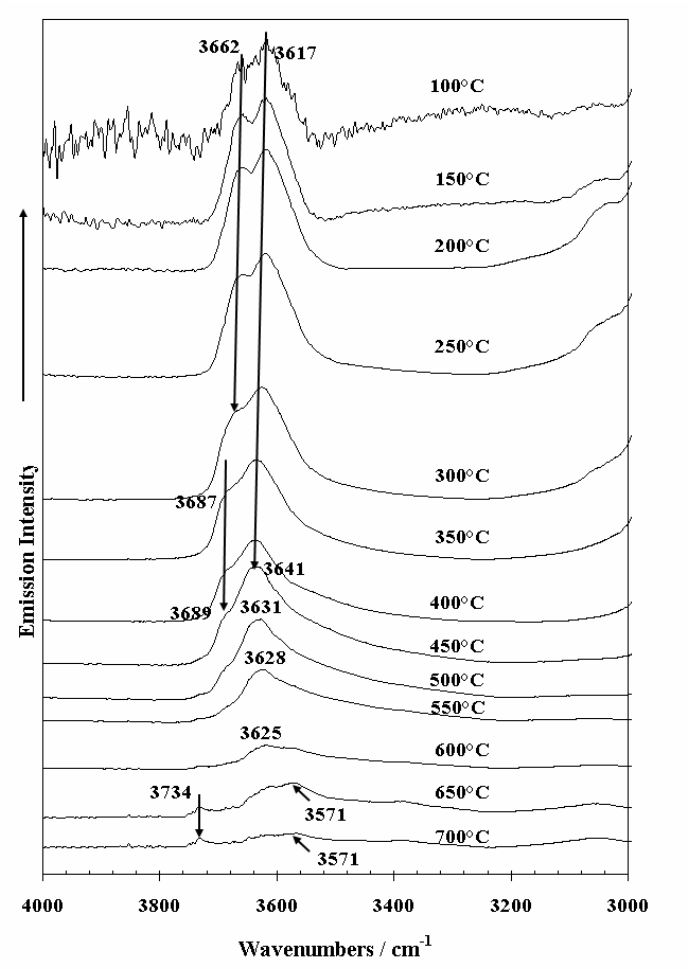
3662
3617
100°C
150°C
200°C
250°C
300°C
3687
350°C
3641
3689
3631
400°C
450°C
3628
500°C
550°C
3625
600°C
3734
650°C
3571
700°C
3571
Emission Intensity
4000
3800
3600
3400
3200
3000
Wavenumbers / cm-1

Figure 5c

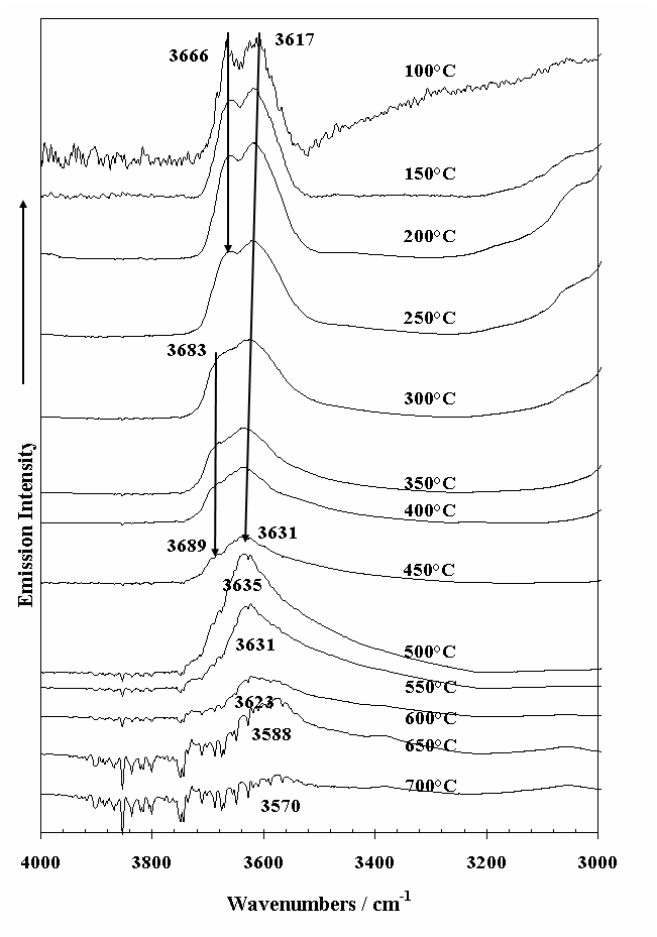
3666
3617
100°C
150°C
200°C
250°C
3683
300°C
350°C
400°C
3689
3631
450°C
3635
3631
500°C
550°C
3623
600°C
3588
650°C
700°C
3570
Emission Intensity
4000
3800
3600
3400
3200
3000
Wavenumbers / cm-1

Figure 5d

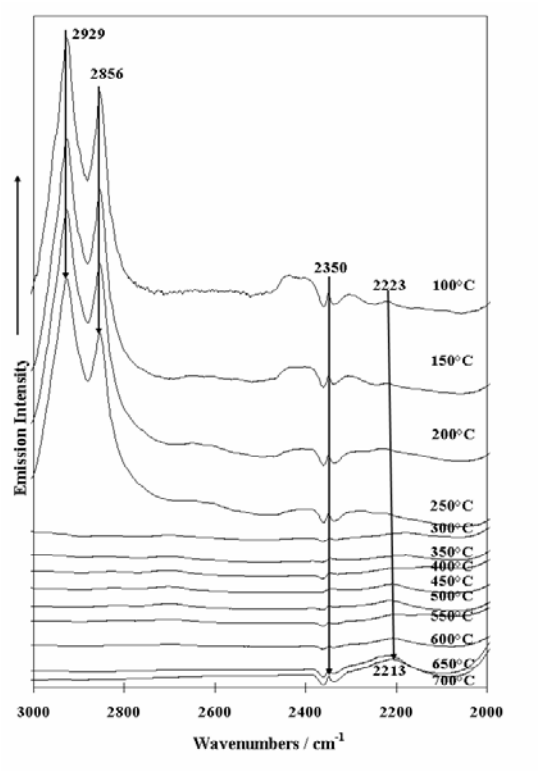

Figure 6a Mt-4000

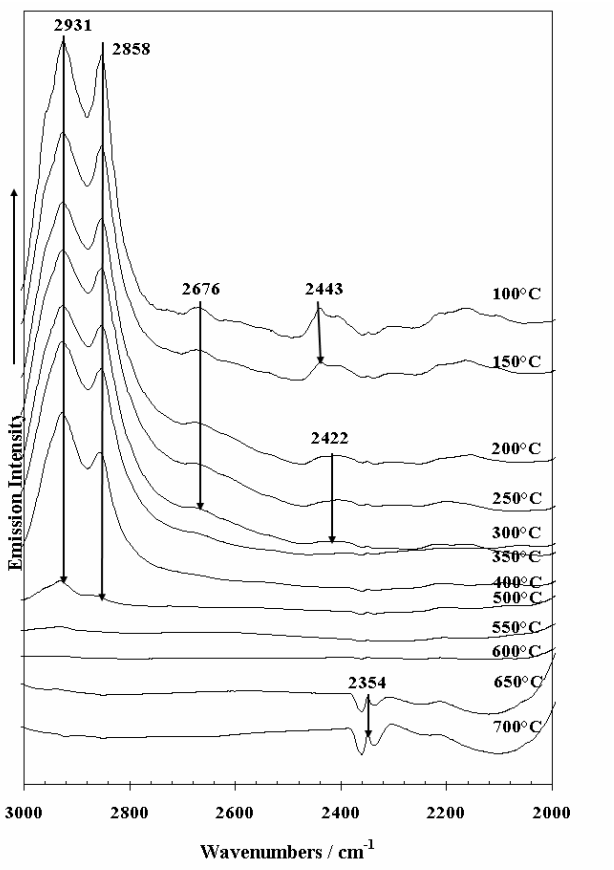
2931
2858
2676
2443
2422
2354
100°C
150°C
200°C
250°C
300°C
350°C
400°C
500°C
550°C
600°C
650°C
700°C
Emission Intensity
3000
2800
2600
2400
2200
2000
Wavenumbers / cm-1

Figure 6b

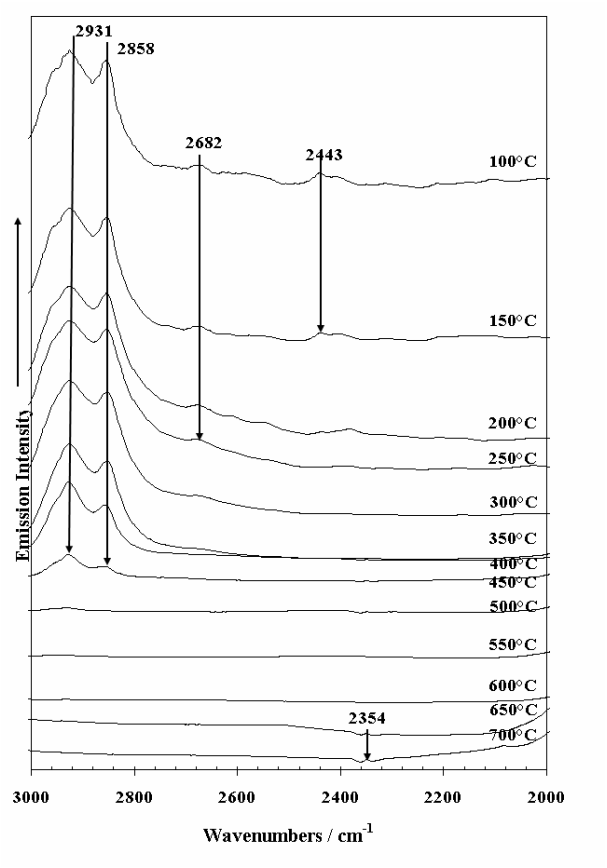
2931
2858
2682
2443
100°C
150°C
200°C
250°C
300°C
350°C
400°C
450°C
500°C
550°C
600°C
650°C
700°C
2354
Emission Intensity
3000
2800
2600
2400
2200
2000
Wavenumbers / cm-1

Figure 6c

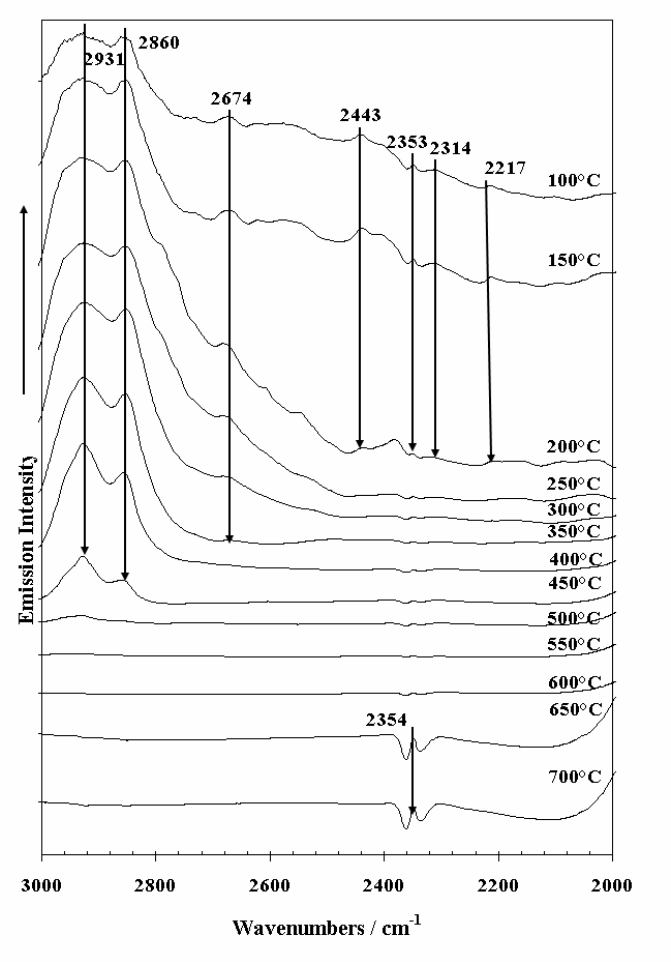
2931
2860
2674
2443
2353
2314
2217
100°C
150°C
200°C
250°C
300°C
350°C
400°C
450°C
500°C
550°C
600°C
650°C
2354
700°C
Emission Intensity
3000
2800
2600
2400
2200
2000
Wavenumbers / cm-1

Figure 6d

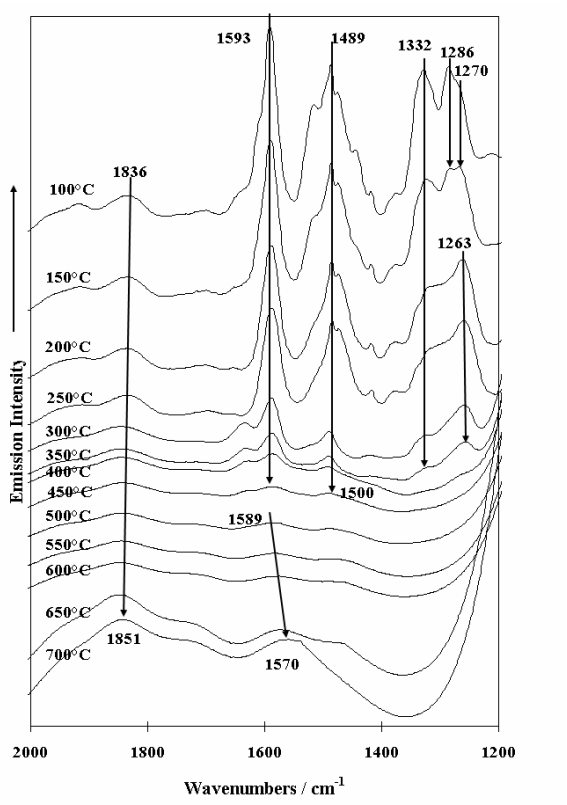

Figure 7a Mt-4000

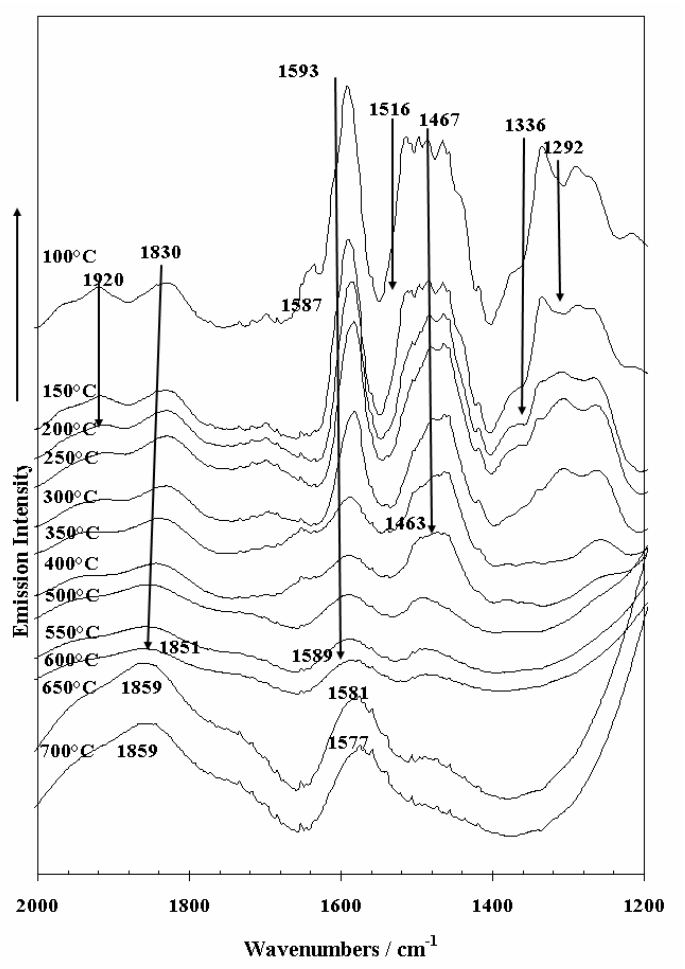
1593
1516
1467
1336
1292
100°C
1830
1920
1587
150°C
200°C
250°C
300°C
350°C
400°C
500°C
550°C
600°C
650°C
700°C
1463
1851
1589
1859
1581
1859
1577
Emission Intensity
2000
1800
1600
1400
1200
Wavenumbers / cm-1

Figure 7b

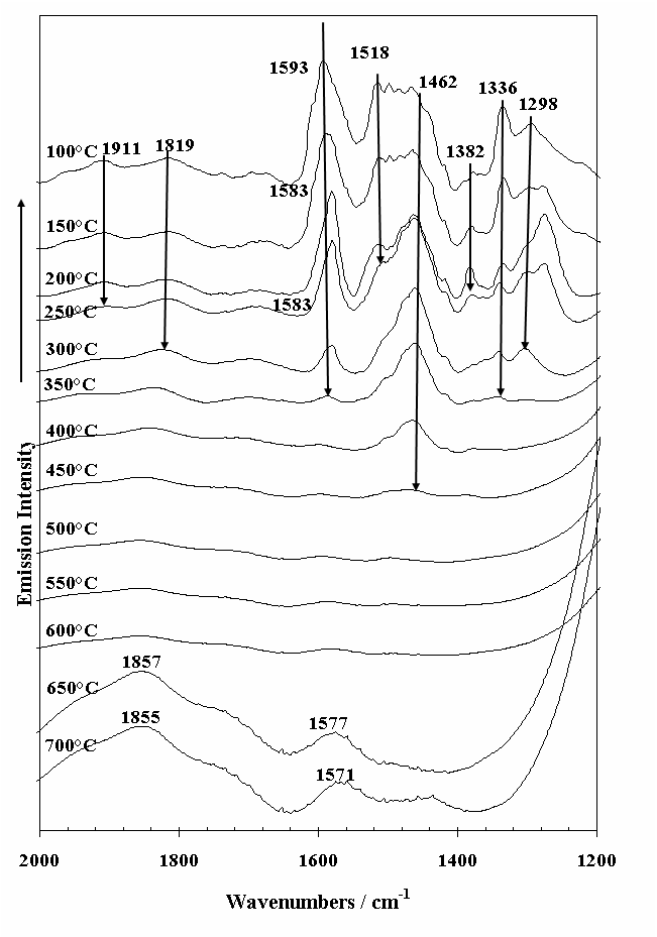
1593
1518
1462
1336
1298
1382
1911
1819
1583
1583
100°C
150°C
200°C
250°C
300°C
350°C
400°C
450°C
500°C
550°C
600°C
650°C
700°C
1857
1855
1577
1571
Emission Intensity
2000
1800
1600
1400
1200
Wavenumbers / cm-1

Figure 7c

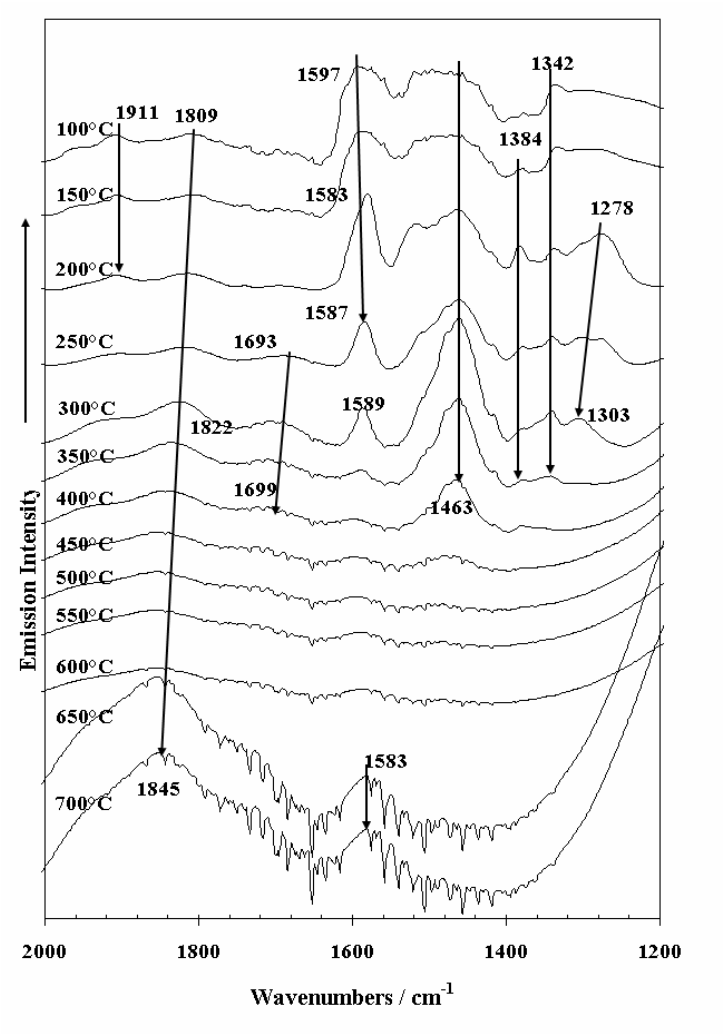
1597
1342
1911
1809
100°C
1384
150°C
1583
1278
200°C
1587
250°C
1693
300°C
1589
1303
1822
350°C
400°C
1699
1463
450°C
500°C
550°C
600°C
650°C
1583
1845
700°C
Emission Intensity
2000
1800
1600
1400
1200
Wavenumbers / cm-1

Figure 7d

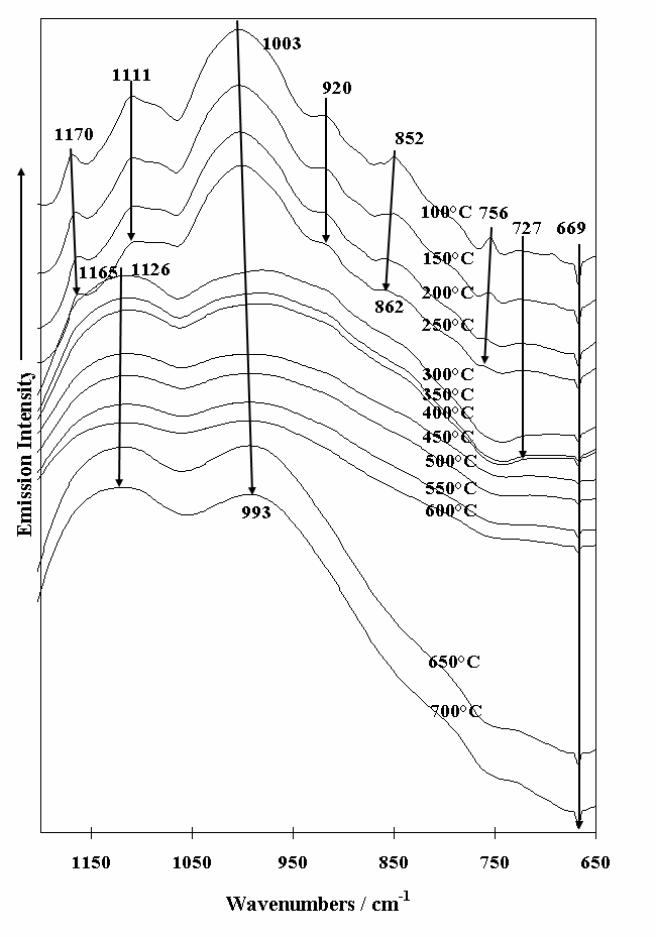

Figure 8a Mt-4000

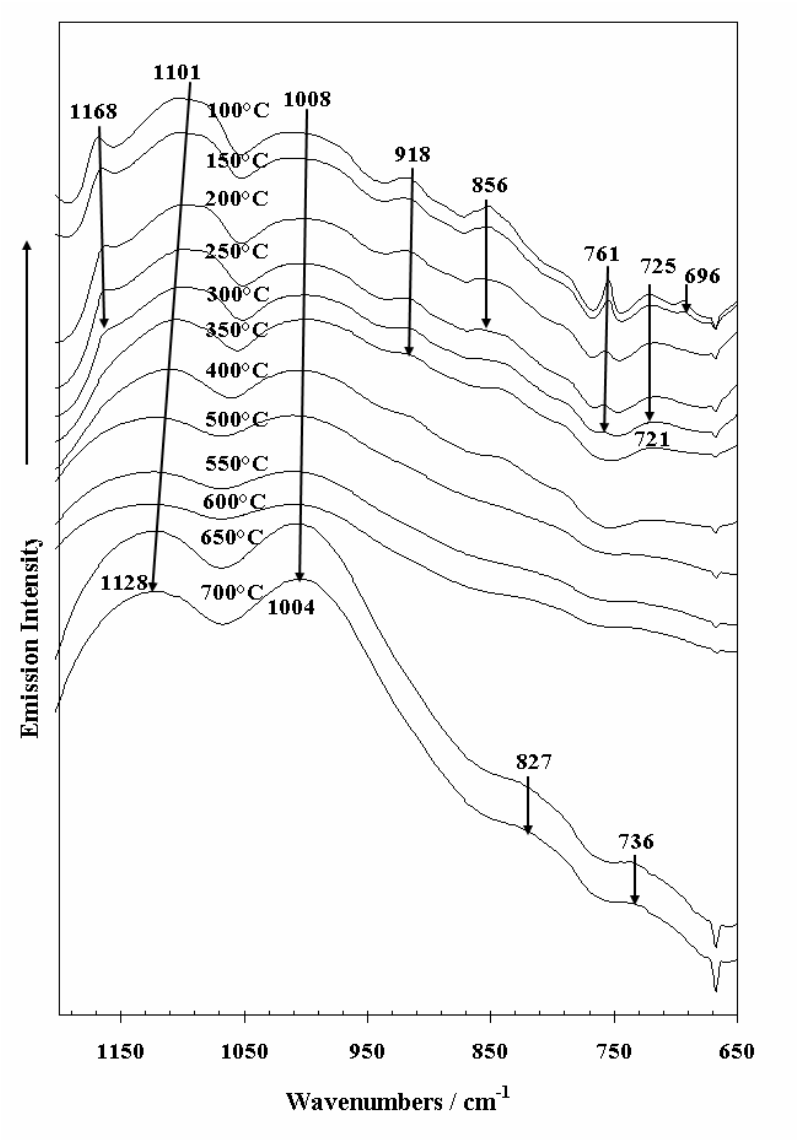
1101
1168
100°C
1008
150°C
918
856
200°C
761
725
696
250°C
300°C
350°C
400°C
500°C
721
550°C
600°C
650°C
1128
700°C
1004
827
736
Emission Intensity
1150
1050
950
850
750
650
Wavenumbers / cm-1

Figure 8b

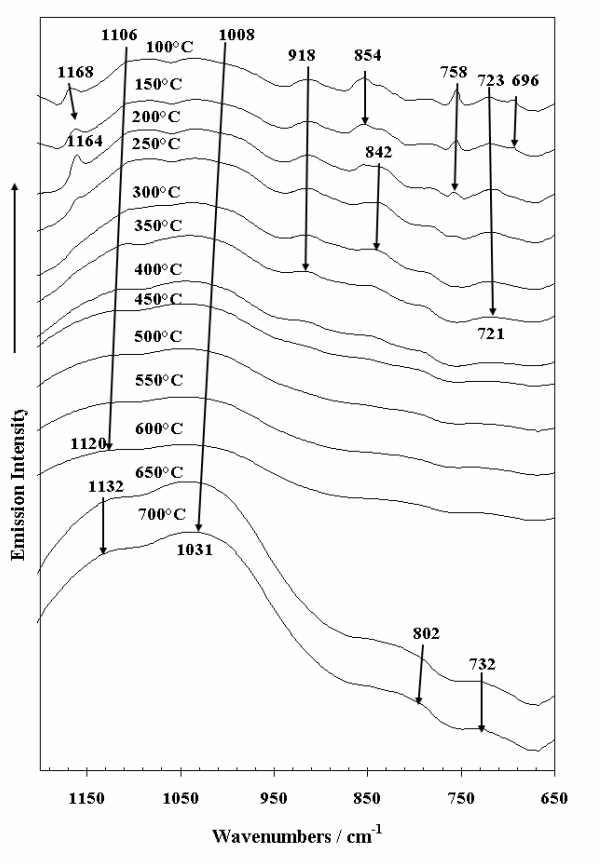
1106
100°C
1008
1168
150°C
918
854
758
723
696
200°C
1164
250°C
842
300°C
350°C
400°C
450°C
721
500°C
550°C
600°C
1120
650°C
1132
700°C
1031
802
732
Emission Intensity
1150
1050
950
850
750
650
Wavenumbers / cm-1

Figure 8c

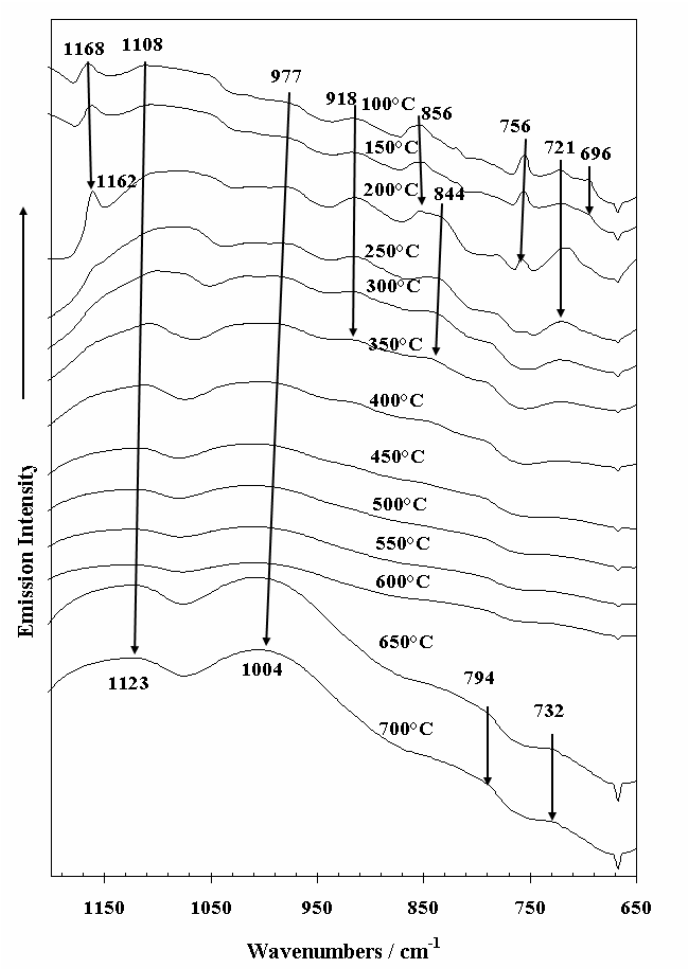
1168
1108
977
918
100°C
856
756
721
696
150°C
1162
200°C
844
250°C
300°C
350°C
400°C
450°C
500°C
550°C
600°C
650°C
794
732
700°C
1123
1004
Emission Intensity
1150
1050
950
850
750
650
Wavenumbers / cm-1

Figure 8d